Neutrosophic segementaion of breast lesions for dedicated breast CT

Juhun Lee*[a], Robert M. Nishikawa[a], Ingrid Reiser[b], John M. Boone[c]
[a] Dept. of Radiology, University of Pittsburgh, 3362 Fifth Ave, Pittsburgh, Pennsylvania, USA 15213; [b]Dept. of Radiology, University of Chicago, 5841 S. Maryland Ave, Chicago, Illinois, USA 60637; [c]Dept. of Radiology, University of California Davis Medical Center, 4860 Y St, Sacramento, California, USA 95817

ABSTRACT

We proposed the neutrosophic approach for segmenting breast lesions in breast Computer Tomography (bCT) images. The neutrosophic set (NS) considers the nature and properties of neutrality (or indeterminacy), which is neither true nor false. We considered the image noise as indeterminate component, while treating the breast lesion and other breast areas as true and false components. We first transformed the image into the NS domain. Each voxel in the image can be described as its membership in True, Indeterminate, and False sets. Operations α-mean, β-enhancement, and γ-plateau iteratively smooth and contrast-enhance the image to reduce the noise level of the true set. Once the true image no longer changes, we applied one existing algorithm for bCT images, the RGI segmentation, on the resulting image to segment the breast lesions. We compared the segmentation performance of the proposed method (named as NS-RGI) to that of the regular RGI segmentation. We used a total of 122 breast lesions (44 benign, 78 malignant) of 123 non-contrasted bCT cases. We measured the segmentation performances of the NS-RGI and the RGI using the DICE coefficient. The average DICE value of the NS-RGI was 0.82 (STD: 0.09), while that of the RGI was 0.8 (STD: 0.12). The difference between the two DICE values were statistically significant (paired t test, p-value = 0.0007). We conducted a subsequent feature analysis on the resulting segmentations. The classifier performance for the NS-RGI (AUC = 0.8) improved over that of the RGI (AUC = 0.69, p-value = 0.006).

Keywords: Neutrosophy, segmentation, quantitative feature analysis, breast CT, CADx

1. INTRODUCTION

In image segmentation problems, the main goal is to distinguish the foreground from the background in the given image. However, all natural images (i.e., not simulated or computer-generated) include various types of noise, which are neither foreground nor background in segmentation problems. Such noises degrade the segmentation performance of any existing segmentation algorithms.

In dedicated breast computer tomography (bCT), quantum noise is one the major source of noises in bCT images. It creates salt and pepper like noise in reconstructed bCT images which can degrade any segmentation algorithms. One can reduce quantum noise by increasing radiation dose. However, we need to limit the amount of radiation dose on patients as it may increase the cancer risk. Thus, one needs to balance the image quality (or image noise) and radiation dose, to maximize the patient benefits (e.g., detection of cancer).

There exist many ways to control the noise in bCT images. One can use different reconstruction kernels e.g., smooth kernels for low noise but low spatial resolution, or sharp kernels for high noise but high spatial resolution. Recently, researchers are developing iterative image reconstruction algorithms for bCT [1,2], which can suppress the image noise while maintain the spatial resolution and contrast even in low radiation dose settings. In addition to these noise controls in the reconstruction domain, we can reduce image noise after reconstruction, directly on bCT images. One may simply smooth the entire image or region of interest of the image to reduce the effect of the noise. However, simply smoothing can remove useful information (e.g., edge of lesion) for segmentation. In this respect, it is beneficial to develop algorithms that suppress image noise while preserving useful information for segmentation.

*jlee15@upmc.edu; phone 1-412-641-2365; fax 1-412-641-2582

This study attempted to distinguish and suppress the noise in the image after reconstruction, before applying the segmentation algorithms. Then, any segmentation algorithms can be applied to noise-suppressed (or cleaner) images to improve segmentation performance. For this study, we adopted neutrosophy theory to achieve the above objective.

Neutrosophy is a branch of philosophy that generalizes dialectics and studies the concept and properties of neutralities[3]. Neutrosophy theory considers entity <A> and its relation to <Anti-A> and <Neut-A>, where <Anti-A> and <Neut-A> represent the opposite and the neutrality entity of <A>, respectively. Neutrosophy covers various concepts, including neutrosophic logic, neutrosophic probability, nuetrosophic set, etc[3]. One can consider neutrosophy logic as the generalized version of fuzzy logic, where it explicitly takes into account the neutrality or indeterminacy of the problem[4].

We can consider the noise in the image as a neutral or indeterminate element. The classical set and fuzzy set only handle this neutral or indeterminate element partially, as neutrality or indeterminacy is absorbed into either the true or false set (or background or foreground set). Due to the existence of neutrality, one can expect that the neutrosophy set can handle the noise element in the image effectively.

This study, therefore, used the neutrosophy theory, specifically the neutrosophic set, to tackle segmentation problems for dedicated breast CT images. This study adapted and modified the segmentation approach proposed by Guo and Cheng[5] to solve our problem, i.e., segmenting breast lesion in bCT images. The method of Guo and Cheng started from transforming the given image into the neutrosophy set (NS) domain. Then, two operations called α-mean and β-enhancement are applied to the resulting image iteratively to *clean* the foreground image by segregating foreground, noise, and background into true, indeterminant, false set in NS domain. The original method was used for segmenting breast lesions in 2D Ultrasound images[6]. We extended and modified their method to segment 3D bCT images. Once the reconstructed image is *enhanced* or *cleaned* via the proposed method, we used an existing algorithm to segment breast lesion in bCT image. Then, we compared the segmentation performance of the existing algorithm with and without the proposed noise reduction method. In addition, we conducted quantitative feature analysis (i.e., training/testing a classifier using quantitative image features from the lesion) to further show if the proposed method allows the improvement in classification performance of the trained classifier.

2. METHODS

2.1 Dataset

We used a dataset of 122 pathology proven breast lesions (44 malignant, 78 benign) of 123 non-contrast bCT cases, which was consolidated under an approved Institutional Review Board (IRB) protocol. The prototype dedicated breast CT system at the University of California at Davis[7] was utilized to obtain all patients' bCT cases. This study used a clinical reconstruction algorithm[8] to reconstruct each image. The voxel size of each reconstructed image varies from 190 by 190 to 430 by 430 with coronal slice spacing ranged from 190 to 770 um. The mean voxel sizes are approximately 340 by 340 by 260 um with the standard deviation of 40 by 40 by 80 um. Table 1 summarizes the detailed characteristics of the dataset, which include patient age, lesion size, breast density, and lesion diagnosis.

2.2 Preprocessing

To reduce false positives, we preprocessed bCT images such that they are within the range of the possible voxel intensity of breast tissues. We assumed that the range of Hounsfield unit (HU) of breast tissue as [-500, 300] HU. -500 HU and 300 HU are the highest HU number for lung[9] and the lowest HU number for cortical bone[10], respectively. In fact, previous study[11] showed that Hounsfield unit (HU) values for breast tissue in bCT images can be ranged from -350 (adipose tissue at low kVp) to 100 (breast cancer at high kVp). Another study[12] showed that contrast can enhance malignant breast lesion in bCT images up to 120 HU. Thus, we can expect that the range [-500, 300] HU should include all possible values for breast tissue in bCT images. Any voxels outside of this HU range were replaced with the averaged HU value of other neighboring voxels.

Table 1. Characteristics of Image Dataset. Abbreviations used in this table include, IDC: Invasive Ductal Carcinoma, IMC: Invasive Mammary Carcinoma, ILC: Invasive lobular Carcinoma, DCIS: Ductal Carcinoma In Situ, FA: Fibroadenoma, FC: Fibrocystic, FCC: Fibrocystic changes, PASH: Pseudoangiomatous stromal hyperplasia, CAPPS: columnar alteration with prominent apical snouts and secretions.

Total number of lesions			All
			122
Subject Age [years]		Mean [min, max]	55.6 [35, 80]
Lesion diameter [mm]		Mean [min, max]	13.8 [4, 35]
Breast Density (% among lesions considered)		1	12 (10%)
		2	46 (38%)
		3	46 (38%)
		4	18 (14%)
Diagnosis*	Malignant (% among malignant lesions considered)	IDC	55 (71%)
		IMC	11 (14%)
		ILC	7 (9%)
		DCIS	4 (5%)
		Lymphoma	1 (1%)
	Benign (% among benign lesions considered)	FA	18 (41%)
		FC	7 (16%)
		FCC	4 (9%)
		PASH	1 (2%)
		CAPPS	2 (4%)
		Other benign lesions such as sclerosing adenosis and cyst	12 (28%)

2.3 Neutrosophic image enhancement for breast CT images

Let x(t,i,f) be an element of the neutrosophic set (NS). t, i, and f refer to the membership (%) of the element x in the neutrosophic components; true (T), indeterminacy (I), and false (F), respectively. In this study, we treated T, I, and F as foreground, noise, and background, respectively.

Let V(x, y, z) be the voxel of the bCT image. Neutrosophic representation of V(x, y, z) is given as $V_{NS}(x, y, z) = \{T(x, y, z), I(x, y, z), F(x, y, z)\}$, where each neutrosophic component is defined as the following equations,

$$T = \frac{p_w - \min(p_w)}{\max(p_w) - \min(p_w)},\ I = \frac{p_g - \min(p_g)}{\max(p_g) - \min(p_g)},\ F = 1 - T, \qquad \text{(Eq 1)}$$

where p is the intensity level of V(x, y, z), and $p_w = meanfilt(p, w)$, represents the mean filtering of the image with the cubic window size of *w* by *w* by *w*, and $p_g = |p - p_w|$. We set *w* as 3 for this step.

The α-mean operation, $V_{NS}^{\alpha}(x,y,z) = V_{NS}\{T^{\alpha}(x,y,z), I^{\alpha}(x,y,z), F^{\alpha}(x,y,z)\}$, is defined as

$$T^{\alpha} = \begin{cases} T, & I < \alpha \\ T_w, & I \geq \alpha \end{cases},\ F^{\alpha} = \begin{cases} F, & I < \alpha \\ F_w, & I \geq \alpha \end{cases},\ I^{\alpha} = \frac{T^{\alpha}{}_g - \min(T^{\alpha}{}_g)}{\max(T^{\alpha}{}_g) - \min(T^{\alpha}{}_g)}, \qquad \text{(Eq 2)}$$

where subscript *w* represents *meanfilt*(. , *w*), and $T^{\alpha}{}_g = |T^{\alpha} - T_w|$. If the indeterminacy level of a voxel is higher than α, the α-mean operation locally smooths the portion around that voxel. We set α and *w* as 0.9 and 3.

The β-enhancement operation, $V_{NS}^{\beta}(x,y,z) = V_{NS}\{T^{\beta}(x,y,z), I^{\beta}(x,y,z), F^{\beta}(x,y,z)\}$, is defined as

$$T^{\beta} = \begin{cases} T, & I < \beta \\ e_{\beta}(T), & I \geq \beta \end{cases},\ F^{\beta} = \begin{cases} F, & I < \beta \\ e_{\beta}(F), & I \geq \beta \end{cases},\ I^{\beta} = \frac{T^{\beta}{}_g - \min(T^{\beta}{}_g)}{\max(T^{\beta}{}_g) - \min(T^{\beta}{}_g)}, \qquad \text{(Eq 3)}$$

where $e_\beta(p) = \begin{cases} 2p^2, & p \le 0.5 \\ 1-2(1-p)^2, & p > 0.5 \end{cases}$, and $T_g^\beta = \left| T^\beta - meanfilt\left(T^\beta, w\right) \right|$.

The β-enhancement operation enhances the contrast of the given volumetric image by reducing the intensity level of a voxel when its corresponding indeterminacy level is higher than β. We set β and *w* as 0.5 and 3.

The γ-plateau operation, $V_{NS}^\gamma(x,y,z) = V_{NS}\left\{T^\gamma(x,y,z), I^\gamma(x,y,z), F^\gamma(x,y,z)\right\}$, is defined a

$$I' = \frac{\left|T_w - \Delta T\right| - \min\left(\left|T_w - \Delta T\right|\right)}{\max\left(\left|T_w - \Delta T\right|\right) - \min\left(\left|T_w - \Delta T\right|\right)},\ T_w = meanfilt(T,w),\ T^\gamma = T,\ F^\gamma = F, \qquad \text{(Eq 4)}$$

where Δ is Laplace operator. The γ-plateau operation is a new addition to the original NS approach proposed by Guo and Cheng, where it changes the indeterminacy set as the edge-enhanced image. When it combines with α-mean operation, it smooths the volume surrounding the given voxel, when it is higher than α. As a result, α-mean operation with γ-plateau operation smooths the peaks and valleys in the foreground and, therefore, creates the plateaued (i.e., smoothed) foreground. We set *w* as 3.

Once the true (i.e., T or foreground), indeterminacy (i.e., I or noise), and false (i.e., F or background) components of the given image in the NS domain no longer changes, which is measured by the sum of entropies of true, indeterminacy, and false sets, $V_{NS}(x, y, z)$ is transformed back to V(x, y, z) with (λ, *w*) = (0.5, 3) as,

$$V = \begin{cases} T, & I \le \lambda \\ T_w, & I > \lambda \end{cases},\ T_w = meanfilt(T,w). \qquad \text{(Eq 5)}$$

We set the threshold for stop the enhancement as 0.0001. Figure 1 shows the diagram explaining the procedure of NS enhancement for bCT images, and Figure 2 shows the effect of NS enhancement on an example bCT image.

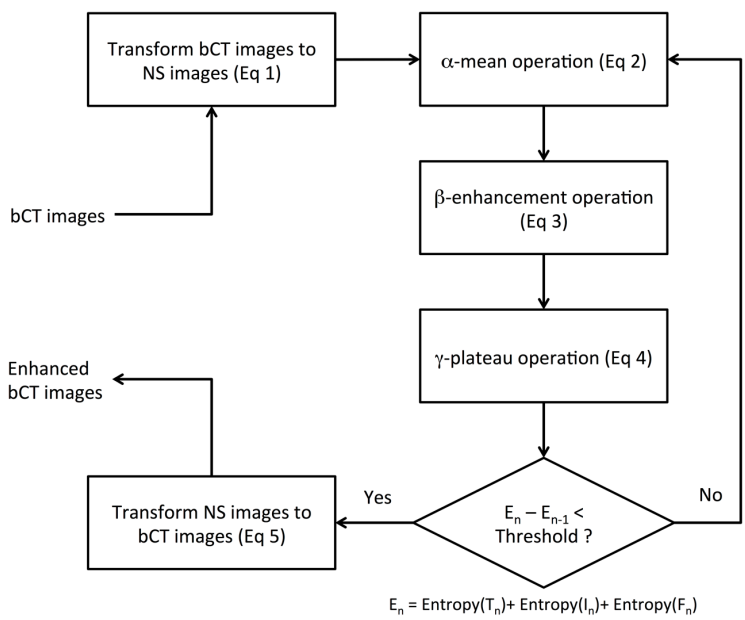

Figure 1. This diagram illustrates the procedures for the proposed Nuetrosophic image enhancement for bCT images. The algorithm transforms the bCT images into NS domain by assigning each voxel's membership in true (foreground), false (background), and indeterminacy (noise) sets. After that, three operations iteratively smooth and enhance the NS image to increase the contrast between true (breast lesion) and false (other breast tissue) sets by isolating image noise. Once the change in true, intermediate, and false sets are stabilized, the algorithm transforms the NS images back to create cleaned or enhanced bCT images.

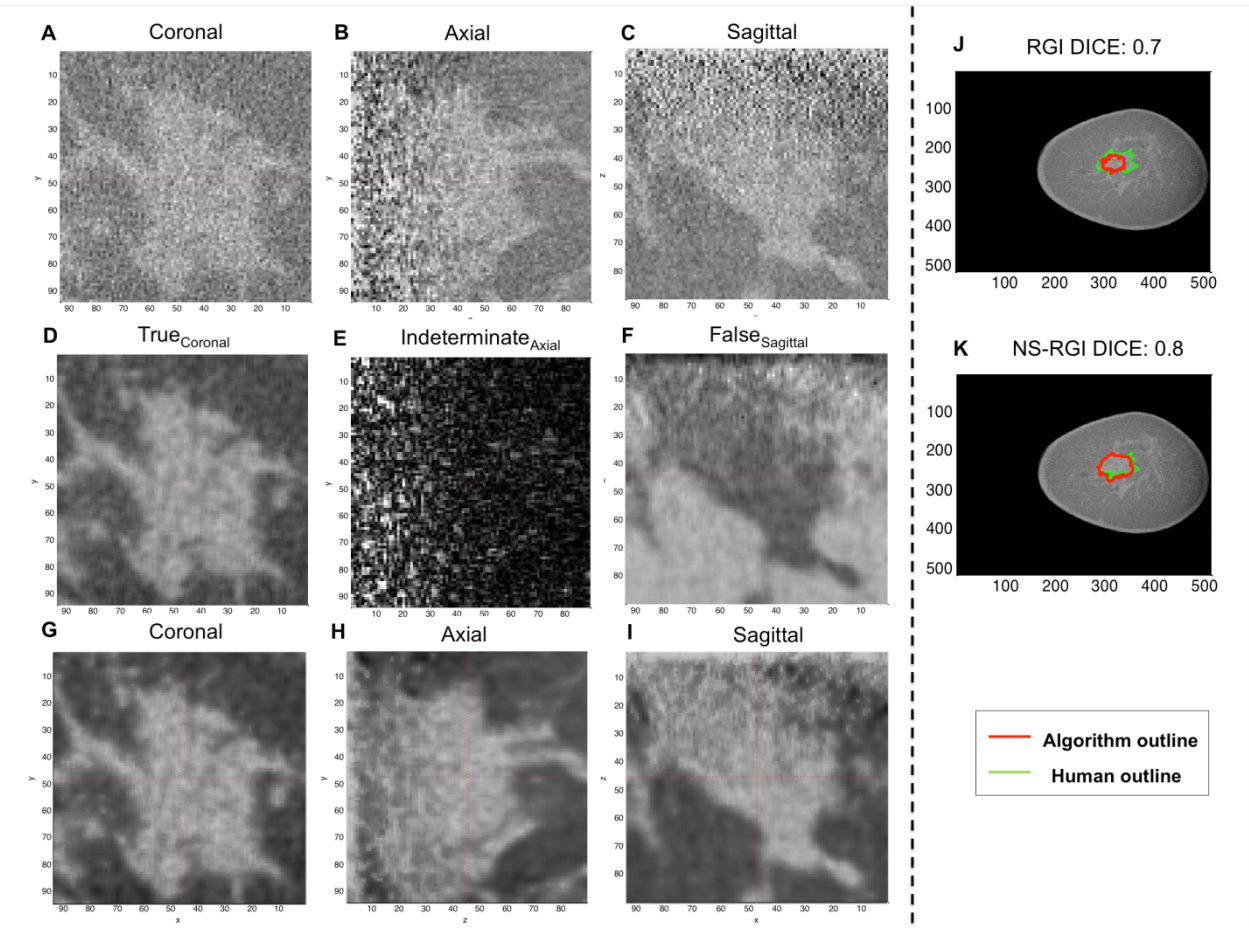

Figure 2. This figure illustrates how the proposed method enhances or cleans the given image for segmentation. **A-C**: input image in coronal, axial, and sagittal view. **D-F**: Images in NS domain after one iteration. **G-I**: output image in coronal, axial, and sagittal view. **J-K**: segmentation results in coronal view for NS-RGI and RGI. It is clear that the NS method was able to clean the noise from the image, while retaining other information (e.g., lesion edge information) in the image, thus resulted in better segmentation.

2.4 Quantitative image feature analysis

Then, we can apply any segmentation algorithms on the resulting cleaned image. In this study, we used the RGI segmentation algorithm[13], which is a semi-automatic algorithm that requires a manually allocated lesion center to search the boundary of that lesion. It was shown that the RGI segmentation algorithm can successfully segment breast lesions in bCT images. We will call this segmentation approach NS-RGI.

We then conducted quantitative feature analysis to determine if the cleaned image and the associated improved segmentation actually resulted in improving classification. We extracted 23 quantitative image features from segmented lesion images, which we used in previous studies on breast CT[14–16]. Using the leave-one-out cross-validation (LOOCV), we selected the most salient features for classifying breast lesions using a feature selection algorithm. Then, we trained and tested the logistic regression classifier within the same LOOCV loop. We used the area under the receiver operating curve (AUC) as a figure of merit. We compared the AUC values of the classifier trained on NS-RGI segmented images and those of RGI segmented images.

3. RESULTS

Mean and standard deviation of DICE coefficients for the NS-RGI algorithm and the regular RGI algorithm were [0.8, 0.12] and [0.82, 0.09], respectively. The difference between the DICE values of the NS-RGI and RGI was statistically significant (paired t-test, p-value = 0.0006). The AUC values for NS-RGI and RGI obtained from LOOCV were 0.8 (95% CI: [0.73, 0.88]) and 0.69 (95% CI: [0.6 0.78]), respectively (Table 2). We estimated the 95% confidence interval for AUC values of both NS-RGI and RGI cases using a statistical method by Delong et al.[17]. The difference in AUC values of NS-RGI and RGI was 0.11 with 95% CI of [0.032 0.19]. The differences between two AUC values were statistically significant with the p-value of 0.006.

Table 2. Classification performance of trained LDA classifiers using LOOCV for NS-RGI and RGI.

Performance Comparison (AUC)		Difference in AUC	
NS-RGI	RGI	$AUC_L - AUC_R$ [95% CI]	*p*-value
AUC_L [95% CI]	AUC_R [95% CI]		
0.8 [0.73, 0.88]	0.69 [0.6, 0.78]	0.11 [0.032, 0.19]	0.006

4. CONCLUSION

This study proposed a new approach to segment breast lesions in bCT images. Its segmentation and associated classification performances are statistically better than the previous method. Although we only tested the method on one segmentation algorithm, it can be worked as a preprocessing step, such that it can be combined with other segmentation algorithms. Further research with larger datasets is required to extend our finding to other imaging modalities, such as MRI.

5. ACKNOWLEDGMENTS

This work has been supported in part by grants from the National Institutes of Health R21-EB015053 and R01-CA181081.

REFERENCES

[1] Antropova, N., Sanchez, A., Reiser, I., Sidky, E. Y., Boone, J. M.., Pan, X., "Efficient iterative image reconstruction algorithm for dedicated breast CT," Proc SPIE 9783 Med. Imaging 2016 Phys. Med. Imaging **9783** (2016).

[2] Sidky, E. Y.., Pan, X., "Image reconstruction in circular cone-beam computed tomography by constrained, total-variation minimization," Phys. Med. Biol. **53**(17), 4777 (2008).

[3] Smarandache, F., A Unifying Field in Logics: Neutrosophic Logic. Neutrosophy, Neutrosophic Set, Neutrosophic Probability, American Research Press, Rehoboth N.M. (2003).

[4] Zhang, M., Zhang, L.., Cheng, H. D., "A neutrosophic approach to image segmentation based on watershed method," Signal Process. **90**(5), 1510–1517 (2010).

[5] Guo, Y.., Cheng, H. D., "New neutrosophic approach to image segmentation," Pattern Recognit. **42**(5), 587–595 (2009).

[6] Xian, M., Cheng, H. D.., Zhang, Y., "A Fully Automatic Breast Ultrasound Image Segmentation Approach Based on Neutro-Connectedness," 2014 22nd Int. Conf. Pattern Recognit. ICPR, 2495–2500 (2014).

[7] Lindfors, K. K., Boone, J. M., Newell, M. S.., D'Orsi, C. J., "Dedicated breast computed tomography: the optimal cross-sectional imaging solution?," Radiol. Clin. North Am. **48**(5), 1043–1054 (2010).

[8] Feldkamp, L. A., Davis, L. C.., Kress, J. W., "Practical cone-beam algorithm," J. Opt. Soc. Am. A **1**(6), 612–619 (1984).

[9] Brown, R. H., Wise, R. A., Kirk, G., Drummond, M. B.., Mitzner, W., "Lung Density Changes With Growth and Inflation," Chest **148**(4), 995–1002 (2015).

[10] Naik, M. N., Tourani, K. L., Sekhar, G. C.., Honavar, S. G., "Interpretation of computed tomography imaging of the eye and orbit. A systematic approach," Indian J. Ophthalmol. **50**(4), 339 (2002).
[11] Boone, J. M., Nelson, T. R., Lindfors, K. K.., Seibert, J. A., "Dedicated Breast CT: Radiation Dose and Image Quality Evaluation," Radiology **221**(3), 657–667 (2001).
[12] Prionas, N. D., Lindfors, K. K., Ray, S., Huang, S.-Y., Beckett, L. A., Monsky, W. L.., Boone, J. M., "Contrast-enhanced Dedicated Breast CT: Initial Clinical Experience1," Radiology **256**(3), 714–723 (2010).
[13] Reiser, I., Joseph, S. P., Nishikawa, R. M., Giger, M. L., Boone, J. M., Lindfors, K. K., Edwards, A., Packard, N., Moore, R. H., et al., "Evaluation of a 3D lesion segmentation algorithm on DBT and breast CT images," Proc SPIE 7624 Med. Imaging 2010 Comput.-Aided Diagn., 76242N–76242N–7 (2010).
[14] Lee, J., Nishikawa, R. M., Reiser, I., Boone, J. M.., Lindfors, K. K., "Local curvature analysis for classifying breast tumors: Preliminary analysis in dedicated breast CT," Med. Phys. **42**(9), 5479–5489 (2015).
[15] Kuo, H.-C., Giger, M. L., Reiser, I., Drukker, K., Boone, J. M., Lindfors, K. K., Yang, K.., Edwards, A., "Impact of lesion segmentation metrics on computer-aided diagnosis/detection in breast computed tomography," J. Med. Imaging **1**(3), 031012–031012 (2014).
[16] Reiser, I., Nishikawa, R. M., Giger, M. L., Boone, J. M., Lindfors, K. K.., Yang, K., "Automated detection of mass lesions in dedicated breast CT: a preliminary study," Med. Phys. **39**(2), 866–873 (2012).
[17] DeLong, E. R., DeLong, D. M.., Clarke-Pearson, D. L., "Comparing the Areas under Two or More Correlated Receiver Operating Characteristic Curves: A Nonparametric Approach," Biometrics **44**(3), 837–845 (1988).

View publication stats